NUKLEONIKA 2013;58(2):261–267

ORIGINAL PAPER

Synthesis and *in vivo* evaluation of both (2*R*,3*R*)-[^{123}I]- and (2*S*,3*S*)-[^{123}I]-trans-2-hydroxy-5-((E)-3-(iodo)allyloxy)-3-(4-phenyl-l-piperazinyl) tetralin as SPECT radiotracer

Thaer Assaad, Abdul H. Al Rayyes

Abstract. We report the synthesis of enantiopure benzovesamicol derivatives: (2*R*,3*R*)-[^{123}I]-trans-2-hydroxy-5-((E)-3-(iodo)allyloxy)-3-(4-phenyl-1-piperazinyl) tetralin and (2*S*,3*S*)-[^{123}I]-trans-2-hydroxy-5-((E)-3-(iodo)allyloxy)-3-(4-phenyl-1-piperazinyl) tetralin; [(2*R*,3*R*)-[^{123}I]-1 and (2*S*,3*S*)-[^{123}I]-1]. Both compounds were obtained with radiochemical and optical purities greater than 97% and with radiochemical yields in the range of 50–60%. To determine whether these compounds could have potential advantage compared to [^{125}I]-iodo benzovesamicol (IBVM), IBVM was also labelled and used as the reference compound in all *in vivo* experiments. Both (2*R*,3*R*)-[^{123}I]-1 and (-)-[^{125}I]-IBVM showed similar time activity curves (TACs) with the highest accumulations in the striatum region followed by the cortex, hippocampus and then cerebellum. While (2*S*,3*S*)-[^{123}I]-1 showed an overall homogeneous brain distribution. However, time activity curves of (2*R*,3*R*)-[^{123}I]-1 confirmed that this compound could be used to visualize the vesicular acetylcholine transporter (VAChT) *in vivo*, at each point of the kinetic study. Also (2*R*,3*R*)-[^{123}I]-1 showed lower specific bindings compared to [^{125}I]-IBVM. These results suggested that (2*R*,3*R*)-[^{123}I]-1 is inferior in comparison with [^{125}I]-IBVM for *in vivo* VAChT exploration.

Key words: Alzheimer's disease • benzovisamicol derivatives • brain biodistribution • enantiomeric resolution • radioiodination • vesicular acetylcholine transporter (VAChT)

Introduction

Alzheimer's disease, the most widely known example of a central cholinergic pathology, is characterized by the loss of basal forebrain cholinergic neurons [12], which provide the majority of cholinergic innervations to the cerebral cortical mantle [18]. Radiotracer analogs of benzovesamicol that bind with high affinity to the vesamicol receptor which is located on the uptake transporter of acetylcholine storage vesicles, may provide an *in vivo* marker of cholinergic neuronal integrity. This binding is highly enantioselective and non-competitive with acetylcholine, indicating that the vesamicol receptor allosterically modulates the transporter [1, 5, 6, 14]. A number of benzovesamicol derivatives have been labelled with positron-emitting isotopes and have been used in tomographic imaging of cholinergic nerve density in human brain [7–11, 13–17, 18–20].

We have recently reported the synthesis of the racemic mixture of ^{123}I-(±)-trans-2-hydroxy-5-((E)-3-(iodo)allyloxy)-3-(4-phenyl-1-piperazinyl) tetralin; (2*RS*,3*RS*)-1, which showed lower specific bindings compared with the reference compound (-)-[^{125}I]-IBVM. Time activity curves of (2*RS*,3*RS*)-1 con-

T. Assaad✉, A. H. Al Rayyes
Department of Chemistry,
Atomic Energy Commission of Syria (AECS),
P. O. Box 6091, Damascus, Syrian Arab Republic,
Tel.: +963 11 213 2580, Fax: +963 11 611 2289,
E-mail: cscientific@aec.org.sy

Received: 17 May 2012
Accepted: 12 April 2013

firmed that this compound is inferior in comparison with the reference compound for *in vivo* exploration by SPECT [3]. Moreover it is well known that the specific binding of benzovesamicol derivatives is highly enantioselective, and therefore, working with enantiomerically pure compounds, could improve the compound activity.

In this paper we report the enantiomeric resolution, radiolabelling and preliminary *in vivo* studies in rats of radioiodinated ^{123}I-(2*R*,3*R*) and ^{123}I-(2*S*,3*S*)-trans--2-hydroxy-5-((E)-3-(iodo)allyloxy)-3-(4-phenyl-1--piperazinyl) tetralin obtained from their corresponding n-tributyltin precursors.

Experimental

General remarks

All chemical reagents and solvents were of commercial quality and used as received. [^{125}I]-IBVM was prepared following a reported procedure by iododestannylation of its n-tributyltin precursor, and subsequently synthesized as previously described [17–20]. The thin-layer chromatography technique (TLC) was performed using Merck 60F_{254} silica gel plates. For routine purification of reaction products, flash chromatography was used with silica gel (70–230 mesh). Visualization was accomplished either under UV or in an iodine chamber. NMR spectra were recorded using a Bruker Bio spin 400 spectrometer (400 MHz for ^{1}H, 100 MHz for ^{13}C). Chemical shifts (δ) were expressed in ppm relative to tetramethylsilane (TMS) as an internal standard. IR spectra were recorded using FTIR-JASCO 300E. Melting point determination was performed with a digital melting point instrument from Stuart model SMP3. (2*RS*,3*RS*)-trans-2-hydroxy-5-amino-3-(4-phenyl-1--piperazinyl) tetralin; (2*RS*,3*RS*)-2 was synthesized and labelled with radioiodine-123 from its corresponding n-tributyltin precursors following the same procedure as in the literature [2, 4].

High purity radioiodide-123 produced by proton irradiation of more than 98% enriched xenon-124 inside KIPROS 50 gas target (Karlsruhe Iodine Production System). The nuclear reaction was induced using 30 MeV proton beam extracted from Cyclone-30 cyclotron from Ion Beam Applications. ^{123}INa was produced using KIPROS concentration and purification system. The paper chromatographic analysis was performed using Whatman 3MM paper chromatography strips (2 × 10 cm). The radioactive spot migration was determined by gamma scanner purchased from Bioscan equipped with a sodium iodide detector.

Enantiomeric resolution of (2*RS*,3*RS*)-2 using (+)-CSA

The racemic mixture of (2*RS*,3*RS*)-2 was efficiently separated into its enantiomers by complexation with (1*S*)-(+)-camphor-10-sulphonic acid (+)-CSA (Scheme 1). Briefly, racemic (2*RS*,3*RS*)-2 (500 mg, 1.54 mmol) and (+)-CSA (361.3 mg, 1.54 mmol) were dissolved in boiling acetonitrile. The mixture was stirred at room temperature (r.t.) for 16 h. The precipitate obtained on standing, was filtered and treated with 1 N sodium hydroxide (NaOH) and 25 ml of chloroform ($CHCl_3$). While the supernatant was treated with $CHCl_3$ (3 × 25 ml). The combined organic extracts were washed with saturated brine, dried over anhydrous sodium sulphate Na_2SO_4 and finally evaporated to dryness to obtain (2*R*,3*R*)-2 with 70% overall yield (350 mg, (m.p. 226.5°C), $(\alpha)^{24.7°C}$ = –100.00°). The filtrate was concentrated and the residue was worked up as outlined above to obtain (2*S*,3*S*)-2 with 30% overall yield (150 mg, (m.p. 221.6–222°C), $(\alpha)^{26.8°C}$ = +133.33°.

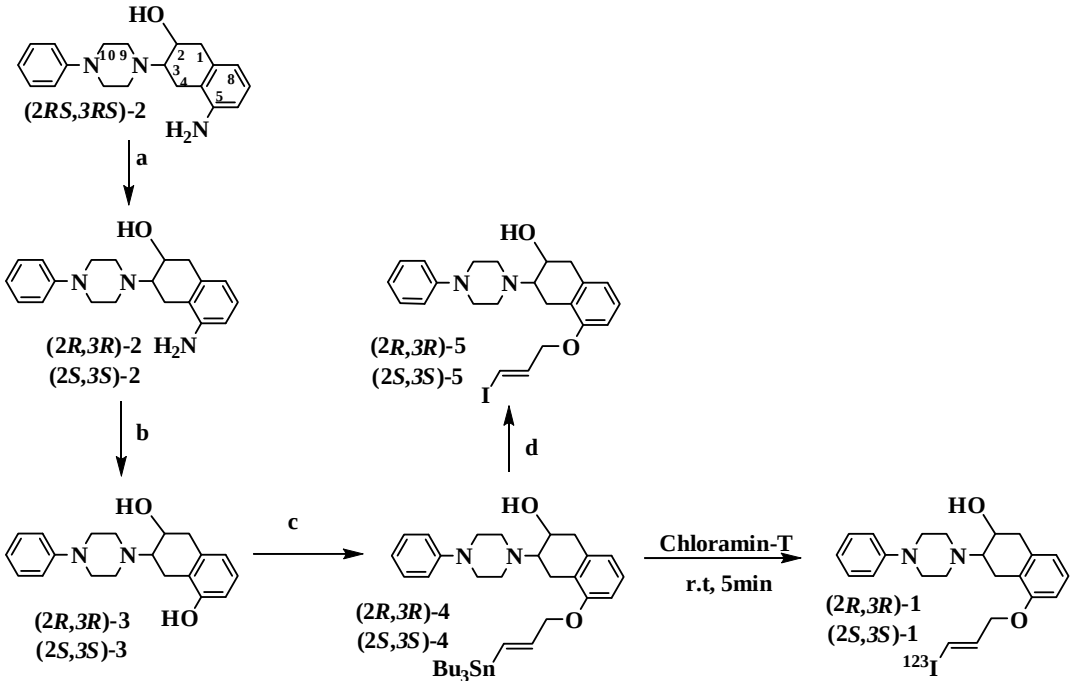

Scheme 1. Synthesis, enantiomeric resolution and radiolabelling of (2*R*,3*R*)-[^{123}I]-1, (2*S*,3*S*)-[^{123}I]-1. Reagents and conditions: (a) (1*S*)-(+)-camphor-10-sulphonic acid (+)-CSA, acetonitrile, r.t., 16 h; (b) THF, H_2SO_4, $NaNO_2$, 5°C; (c) TBAOH, CH_3CN, (E) $Bu_3SnCH{=}CH\text{-}CH_2\text{-}Cl$, 80°C; (d) I_2, $CHCl_3$, – 5°C.

Spectroscopic data of (2R,3R)-2: ^{1}H-NMR ($CDCl_3$)

δ 2.49–2.56 (m, 2H, 2H-10), 2.72–3.31 (m, 12H, 2H-1, 2H-4, 2H-10, 4H-9, H-3, OH), 3.60 (s, NH_2), 3.89–3.94 (m, 1H, H-2), 6.57–6.63 (m, 2H, H-6, H-8), 6.89–6.93 (t, 2H, ^{3}J = 7.2 Hz, $2H_{Ar}$), 6.97–7.04 (m, 1H, H-7), 7.28–7.33 (m, 3H, $3H_{Ar}$). **^{13}C-NMR ($CDCl_3$)**: δ 20.9 (2C--10), 38.0 (C-1), 48.1 (C-4), 49.9 (C-3), 65.2 (C-2), 66.2 (2C-9), 112.7 (CH_{Ar}), 116.3 ($2CH_{Ar}$), 119.3 (C_{Ar}), 119.6 (CH_{Ar}), 120.0 (CH_{Ar}), 127.0 (CH_{Ar}), 129.1 ($2CH_{Ar}$), 134.8 (C_{Ar}), 144.4 (C-NH_2), 151.2 (C_{Ar}). **IR** (KBr, ν cm^{-1}): 3200–3350.4 (N$\underline{H}_2$), 3459.5 (OH), 3050 ($\underline{CH}$=CH, Ar), 2918.2–2850.9 (CH_2, aliphatic), 2850.9 ($\underline{CH_2}$-N), 1636.6 (C=C), 1137.6 (C-N, piperazine).

Synthesis of both (2R,3R) and (2S,3S)-trans-2,5-dihydroxy-3-(4-phenyl-1-piperazinyl) tetralin; (2R,3R)-3 and (2S,3S)-3

A 1:2 dilution of concentrated sulphuric acid in water (5.4 ml) was added to a cooled solution of (2*R*,3*R*)-2 or (2*S*,3*S*)-2 (508 mg, 1.55 mmol) in tetrahydrofuran (THF) (25 ml). A solution of sodium nitrite (130 mg, 5.4 mmol) in water (5.4 ml) was added dropwise at 5°C on stirring for 1 h. The resulting diazonium solution was then added carefully in small aliquots to a boiled sulphuric acid (5.4 ml) in water (28 ml). Subsequently, the mixture was boiled for 15 min and allowed to cool to room temperature. The pH was adjusted to 9 by 5 N NaOH and extracted with ethyl acetate (3 × 50 ml). The combined extracts were dried over anhydrous Na_2SO_4 and concentrated under reduced pressure. The residue was purified by chromatography on silica gel with ethyl acetate (EtOAc):n-Hexane (30:70) to give an overall yield of 340 mg (40%) of (2*R*,3*R*)-3 as a yellow solid and 64% overall yield of (2*S*,3*S*)-3 as a pink solid.

Spectroscopic data of (2R,3R)-3: ^{1}H-NMR ($CDCl_3$)

δ 2.60–3.34 (m, 15H, 4H-9, 2H-4, H-3, H-11, 2H-1, 4H-10, OH), 3.89–3.93 (m, 1H, H-2), 6.51–6.53 (d, 1H, ^{3}J = 8 Hz, H-6), 6.72–6.74 (d, 1H, ^{3}J = 8 Hz, H-8), 6.91–7.34 (m, 6H, H-7, 5H-Ar). **^{13}C-NMR ($CDCl_3$)**: δ 19.9 (2C-10), 37.8 (C-1), 48.0 (C-4), 50.1 (C-3), 65.3 (C-2), 66.1 (2C-9), 112.1 (CH_{Ar}), 116.5 ($2CH_{Ar}$), 120.2 (C_{Ar}), 121.4 (CH_{Ar}), 121.6 (CH_{Ar}), 126.9 (CH_{Ar}), 129.2 ($2CH_{Ar}$), 135.7 (C_{Ar}), 142.1 (C-OH), 153.5 (C_{Ar}). **IR** (KBr, ν cm^{-1}): 3441 (OH, st), 2922, 2962 (CH, aliphatic), 2850 ($\underline{CH_2}$-N).

Synthesis of both (2R,3R) and (2S,3S)-trans-2-hydroxy--5-((E)-3-(tributylstannyl)allyloxy)-3-(4-phenyl-1--piperazinyl) tetralin; (2R,3R)-4 and (2S,3S)-4

Tetrabutylammonium hydroxide (TBAOH) (160 mg) was added to a solution of (2*R*,3*R*)-3 or (2*S*,3*S*)-3 (200 mg, 62 mmol), in dichloromethane (CH_2Cl_2) (20 ml) under inert atmosphere. The solvent was removed under vacuum at room temperature, and the residue was treated twice with dry acetonitrile (CH_3CN) (10 ml) followed each time by rotary evaporation to azeotropically to remove traces of moisture. The mixture was resuspended in dry CH_3CN (10 ml), then (E)-3-chloro--1-tributylstannylprop-2-ene (293.4 mg, 0.8 mmol) was added. The solution was heated, under inert atmosphere at 80°C for 3 h, and then stirred overnight at room temperature. After solvent removing, the crude product was portioned between CH_2Cl_2 and water (20 and 10 ml, respectively) and the organic layer was washed with 0.5 N NaOH, dried over Na_2SO_4, concentrated and purified by flash chromatography on silica gel (EtOAc:n--Hexane, 30:70) to give an overall yield 100 mg (20%) of (2*R*,3*R*)-4 and 66% overall yield of (2*S*,3*S*)-4.

Spectroscopic data of (2R,3R)-4: ^{1}H-NMR ($CDCl_3$)

δ 0.95 (t, 9H, ^{3}J = 7.0 Hz, $3CH_3$), 1.26–1.57 (m, 18H, ($CH_3C\underline{H}_2C\underline{H}_2C\underline{H}_2)_3Sn$), 2.35–2.62 (m, 2H, 2H-10), 2.44–3.19 (m, 12H, H-11, 2H-1, 2H-4, H-3, 4H-9, 2H-10), 3.91–3.93 (m, 1H, H-2), 4.58 (d, 2H, ^{3}J = 4.3 Hz, OCH_2), 6.21–6.38 (m, 2H, -CH=CH-), 6.67–6.54 (m, 8H, $8H_{Ar}$). **^{13}C-NMR ($CDCl_3$)**: δ 9.4 [$(CH_2)_3Sn$], 13.7 ($3CH_3$), 27.2 [$(CH_3\underline{C}H_2CH_2CH_2)_3Sn$], 29.0 [$(CH_3CH_2\underline{C}H_2CH_2)_3Sn$], 34.4 (2C-10), 38.0 (C-1), 42.9 (C-4), 52.5 (C-3), 65.3 (C-2), 66.1 (2C-9), 71.3 (OCH_2), 112.1 (CH_{Ar}), 116.5 ($2CH_{Ar}$), 120.2 (C_{Ar}), 121.4 (CH_{Ar}), 126.9 (CH_{Ar}), 129.2 ($2CH_{Ar}$), 131.1 (SnCH=), 135.7 (C_{Ar}), 153.5 (C_{Ar}), 143.1 (CH=), 146.1 (C_{Ar}), 156.5 (C_{Ar}). **IR** (KBr, ν cm^{-1}): 3421 (OH, m), 2870, 2915, 2955 (CH, $\underline{Bu}_3$), 2850 ($\underline{CH_2}$-N), 1600 (C=C-Sn), 1086 (C-O).

Synthesis of both (2R,3R) and (2S,3S)-trans-2-hydroxy--5-((E)-3-(iodo)allyloxy)-3-(4-phenyl-1-piperazinyl) tetralin; (2R,3R)-5 and (2S,3S)-5

Stannyl derivative (2*R*,3*R*)-4 or (2*S*,3*S*)-4 (50 mg, 76.5 mmol), was dissolved in $CHCl_3$ (5 ml) and cooled at –5°C. A solution of iodine in CH_2Cl_2 (0.1 N) was then added in aliquots, under constant stirring, until a coloured solution was resulted. The reaction mixture was washed with concentrated sodium disulphite ($Na_2S_2O_5$) (5 ml), the organic layer was separated and the aqueous one was extracted with CH_2Cl_2 (3 × 20 ml). The combined organic layers were dried over anhydrous Na_2SO_4 and concentrated. The crude product was purified by flash chromatography on silica gel (EtOAc:n-Hexane, 30:70) to give an overall yield 45% of (2*R*,3*R*)-5 and 40% overall yield of (2*S*,3*S*)-5.

Spectroscopic data of (2R,3R)-5: ^{1}H-NMR ($CDCl_3$)

δ 2.72–2.91 (m, 2H, 2H-10), 2.65–3.32 (m, 12H, H-11, 2H-1, 2H-4, H-3, 4H-9, 2H-10), 4.11–4.30 (m, 1H, H-2), 4.5 (d, 2H, ^{3}J = 4.3 Hz, OCH_2), 6.44–6.58 (m, 2H, -CH=CH-), 6.77–6.87 (m, 8H, $8H_{Ar}$). **^{13}C-NMR ($CDCl_3$)**: δ 34.2 (2C-10), 38.3 (C-1), 42.5 (C-4), 52.1 (C-3), 65.0 (C-2), 65.9 (2C-9), 71.8 (OCH_2), 79.2 (I-CH), 112.2 (CH_{Ar}), 116.3 ($2CH_{Ar}$), 120.5 (C_{Ar}), 121.2 (CH_{Ar}), 126.3 (CH_{Ar}), 129.4 ($2CH_{Ar}$), 135.7 (C_{Ar}), 140.8 (CH=), 153.5 (C_{Ar}), 146.1 (C_{Ar}), 156.5 (C_{Ar}). **IR** (KBr, ν cm^{-1}): 3450 (OH, w), 2922,2960 (CH, aliphatic), 2852 ($\underline{CH_2}$-N), 1087 (C-O), 690 (C=C-I).

General procedure for radiolabelling and purification of both (2*R*,3*R*)-[^{123}I]-I and (2*S*,3*S*)-[^{123}I]-I

(2*R*,3*R*)-[^{123}I]-1 and (2*S*,3*S*)-[^{123}I]-1 were prepared using electrophilic radioiodide stannylation of the tri-n-butyl-

tin precursors. Briefly, 210 μl of ethanolic 0.02 N H_2SO_4 was added to the vial containing 41.81 MBq (1.127 mCi) of $Na^{123}I$ in 20 μl of 0.02 N NaOH, followed by the addition of tin precursor (125 μg in 125 μl of ethanol). The pH of the reaction mixture was monitored (pH = 0–1), and the reaction was initiated by the addition of 50 μl of freshly prepared aqueous chloramine-T trihydrate (15 mg/ml), followed by vigorous shaking for 2 min. Another 50 μl of freshly prepared aqueous chloramine--T trihydrate (15 mg/ml) was added again, followed by vigorous shaking for a further 2 min. The reaction was quenched by the addition of 420 μl of 0.02 N aqueous (ammonia) NH_4OH. The free ^{123}I was eliminated by filtration over a modified ionic exchange column 2 × 10 mm^2 which contains a Biorex resin (200–400 mesh). The labelled product was then concentrated and washed using a C-18 Sep-Pak column, and eluted subsequently from the C-18 Sep-Pak with 2 ml of absolute ethanol. Finally, this solution was diluted with 0.9% normal saline. Radiochemical purity was determined by paper chromatography using ammonium acetate/ethanol 95% (1/1) as eluent. The strips were scanned by a gamma scanner after the separation process.

General biodistribution studies in rats

Experiments in rats were carried out in compliance with appropriate European Community directive guidelines (86/609/EEC). Biodistribution studies were performed in healthy Wistar han rats (male, 200–250 g). Amounts of 0.3 ml of (2*R*,3*R*)-[^{123}I]-1 or (2*S*,3*S*)-[^{123}I]-1 (1.85–2.59 MBq) in 0.9% NaCl/EtOH were administered to rats intravenously via the tail vein. The animals were anaesthetised and sacrificed, routinely 120 min post--intravenous injection (p.i.v.), and selected tissues were taken out. The radioactivity of the brain, and weighted samples of cerebellum, striatum, frontal cortex, and hippocampus, were measured using a GAMMA MÜVEK NK-360 counter. The results were calculated as a percentage of injected dose per gram of tissue (% ID/g ± SD) (Fig. 1). In order to evaluate *in vivo* deiodination of (2*R*,3*R*)-[^{123}I]-1 and (2*S*,3*S*)-[^{123}I]-1, thyroid gland was removed from each animal and its radioactivity was measured.

Cerebral kinetic studies in rats

For kinetic studies, rats were received an intravenous injection of either (2*R*,3*R*)-[^{123}I]-1 or (2*S*,3*S*)-[^{123}I]-1 (1 MBq in 250 μl of EtOH/saline 20/80) and were sacrificed at 30, 60 or 120 min post injection (p.i.) (n = 6 rats per group). Samples of blood and cerebral regions (cerebellum, striatum, frontal cortex and hippocampus) were removed, weighed and their radioactivities were measured. The uptake was expressed as the percentage of injected dose per gram of tissue (% ID/g).

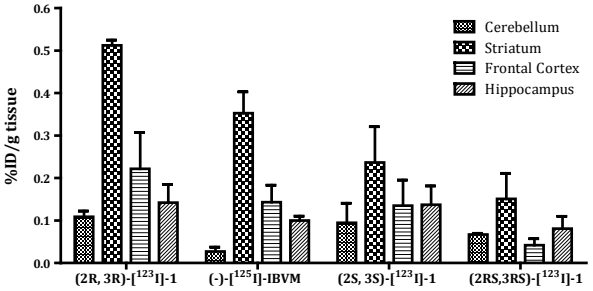

Fig. 1. Cerebral biodistribution of (2*R*,3*R*)-[^{123}I]-1, (2*S*,3*S*)-[^{123}I]-1, (2*RS*,3*RS*)-[^{123}I]-1 and (-)-[^{125}I]-IBVM in the rat (2 h post injection).

Results and discussions

Radiochemistry

Target compounds of (2*R*,3*R*)-[^{123}I]-1 and (2*S*,3*S*)-[^{123}I]-1 (Scheme 1), were prepared using their corresponding n-tributyltin precursor (2*R*,3*R*)-4 or (2*S*,3*S*)-4. The reaction was carried out at room temperature with chloramine-T as an oxidant. Radiochemical purities of the produced radiolabelled compounds were determined by 3MM paper chromatography and found greater than 97%. Radiochemical yields were calculated as non-decay corrected and found in the range of 50–60%.

Cerebral biodistribution studies in rats

Cerebral biodistribution of both (2*R*,3*R*)-[^{123}I]-1 and (2*S*,3*S*)-[^{123}I]-1 were studied in rats and the results were compared to those obtained with (2*RS*,3*RS*)-[^{123}I]-1 and [^{125}I]-IBVM (Fig. 1) [3]. Two hours post injection, (2*R*,3*R*)-[^{123}I]-1 and (2*S*,3*S*)-[^{123}I]-1 have shown different profiles compared to racemic (2*RS*,3*RS*)-[^{123}I]-1.

(2*R*,3*R*)-[^{123}I]-1 showed a good brain penetration with 0.15, 0.22, 0.14% ID/g of tissue in the striatum, cortex and hippocampus, respectively. The striatal binding was found to be higher by a factor of 3.6, 2.3 and 4.7 compared to these of hippocampus, cortex and cerebellum, respectively. The high uptake of (2*R*,3*R*)-[^{123}I]-1 in striatum could be associated with VAChT binding. While, the high concentration found in the cerebellum could be associated with non-specific binding to the VAChT. By contrast; (2*S*,3*S*)-[^{123}I]-1 showed an overall homogeneous brain distribution as no significant difference in activity uptake was measured between the cerebellum and other cerebral regions except the striatum. However, the striatal binding was found to be higher by a factor of 1.72, 1.75 and 2.49 compared to these of hippocampus, cortex and cerebellum regions, respectively. The enantiomeric resolution of the racemic mixture (2*RS*,3*RS*)-1 showed that the analogue (2*R*,3*R*)-1 has higher specific bindings and crossing better the blood brain barrier than the (2*S*,3*S*)-1 and the racemic mixture (2*RS*,3*RS*)-1. This result confirms the fact that the interaction at the VAChT binding sit is enantioselective.

In similar experimental conditions, the reference compound (-)-[^{125}I]-IBVM showed a lower accumulation in the cerebellum (representing the non-specific binding) than in the other studied brain regions with region/cerebellum ratios of 13, 5.29 and 3.7 for the striatum, frontal cortex and hippocampus, respectively (Table 1).

When compared to cerebral biodistribution of (-)-[^{125}I]-IBVM, (2*R*,3*R*)-[^{123}I]-1 displayed a similar

Table 1. Biodistribution (% ID/g of tissue ± SD[a]) of (2*R*,3*R*)-[^{123}I]-1, (2*RS*,3*RS*)-[^{123}I]-1 and (-)-[^{125}I]-IBVM in rat brain

% ID/g	(2*R*,3*R*)-[^{123}I]-1			[^{125}I]-IBVM			(2*RS*,3*RS*)-[^{123}I]-1		
	30 min	60 min	120 min	30 min	60 min	120 min	30 min	60 min	120 min
Cere[b]	0.165 ± 0.076	0.259 ± 0.084	0.108 ± 0.014	0.200 ± 0.020	0.100 ± 0.010	0.027 ± 0.010	0.020 ± 0.016	0.024 ± 0.006	0.051 ± 0.013
Stri[c]	0.264 ± 0.024	0.263 ± 0.027	0.512 ± 0.012	0.530 ± 0.100	0.620 ± 0.010	0.353 ± 0.050	0.033 ± 0.067	0.049 ± 0.020	0.158 ± 0.038
Ctx[d]	0.110 ± 0.046	0.224 ± 0.017	0.221 ± 0.086	0.350 ± 0.080	0.300 ± 0.010	0.143 ± 0.040	0.021 ± 0.005	0.023 ± 0.008	0.032 ± 0.002
Hipp[e]	0.110 ± 0.064	0.211 ± 0.014	0.142 ± 0.043	0.300 ± 0.020	0.240 ± 0.010	0.100 ± 0.010	0.029 ± 0.019	0.032 ± 0.011	0.065 ± 0.008
Thyroid	0.210 ± 0.100	0.630 ± 0.240	0.740 ± 0.140	0.090 ± 0.008	0.120 ± 0.012	0.191 ± 0.030	0.033 ± 0.011	0.067 ± 0.020	0.114 ± 0.078
Stri/cere	1.600 ± 0.187	1.015 ± 0.084	4.740 ± 0.156	2.650 ± 0.141	6.200 ± 0.157	13.074 ± 1.296	1.650 ± 0.900	2.042 ± 0.244	3.098 ± 0.271
Ctx/cere	0.667 ± 0.103	0.864 ± 0.072	2.046 ± 0.209	1.750 ± 0.109	3.000 ± 0.079	5.296 ± 0.614	1.050 ± 0.219	0.958 ± 0.102	0.627 ± 0.041
Hipp/cere	0.667 ± 0.013	0.814 ± 0.067	1.314 ± 0.108	1.500 ± 0.045	2.400 ± 0.065	3.703 ± 0.355	1.450 ± 0.374	1.333 ± 0.141	1.274 ± 0.090

[a]SD – standard deviation.
[b]Cere – cerebellum.
[c]Stri – striatum.
[d]Ctx – cortex.
[e]Hipp – hippocampus.

profile. However, the uptake of (2*R*,3*R*)-[^{123}I]-1 in the cerebellum, which could be considered as non-specific binding, was four times more than IBVM. Thus, regions of interest (ROIs)/cerebellum ratios, which characterize the specific binding, were higher for IBVM compared to (2*R*,3*R*)-[^{123}I]-1 with a maximum striatum/cerebellum ratio of 13 for IBVM vs. 4.7 for (2*R*,3*R*)-[^{123}I]-1.

These results are in agreement with those obtained by Emond *et al*. [8] with (*R*,*R*)-[^{125}I]-AOIBV in rat. They showed that (*R*,*R*)-[^{125}I]-AOIBV has a good brain penetration with 0.22, 0.125, 0.098% ID/g of tissue in striatum, cortex and hippocampus, respectively. Also when compared to cerebral biodistribution of (2*R*,3*R*)-[^{123}I]-1, (*R*,*R*)-[^{125}I]-AOIBV displayed a similar profile. Nevertheless, the uptake of (2*R*,3*R*)-[^{123}I]-1 in the striatum was twice times more than (*R*,*R*)-[^{125}I]--AOIBV. Thus, (ROIs)/cerebellum ratios, were higher for (2*R*,3*R*)-[^{123}I]-1 compared to (*R*,*R*)-[^{125}I]-AOIBV with a maximum striatum/cerebellum ratio of 4.7 for (2*R*,3*R*)-[^{123}I]-1 vs. 4.0 for (*R*,*R*)-[^{125}I]-AOIBV. The presence of piperazine ring in (2*R*,3*R*)-1 instead of piperidine ring in (*R*,*R*)-AOIBV has led to the differences in the *in vivo* biodistribution of the two compounds.

Cerebral kinetic studies in rats

Figures 2, 3 and 4 represent the time activity curves (TACs) of brain regions with different expression levels of VAChT. Both compounds (2*R*,3*R*)-[^{123}I]-1 and (-)-[^{125}I]-IBVM have shown similar TACs with the highest accumulations in the striatum (brain area with high VAChT density) then in the cortex, the hippocampus and finally the cerebellum which was used as a reference region (low VAChT density). While TACs of (2*RS*,3*RS*)--[^{123}I]-1 have shown that the highest accumulations was

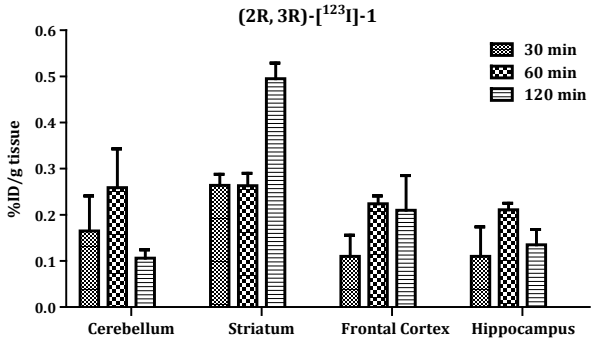

Fig. 2. Kinetic study of (2*R*,3*R*)-[^{123}I]-1 in the rat brain.

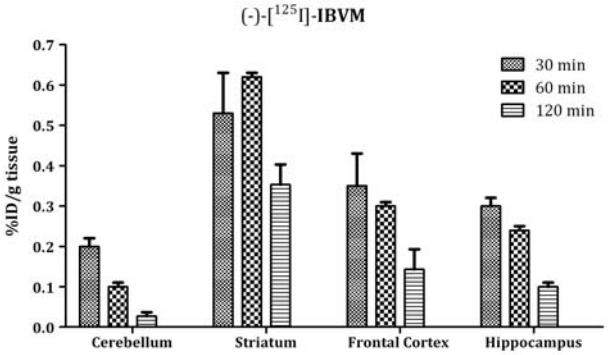

Fig. 3. Kinetic study of (-)-[^{125}I]-IBVM in the rat brain.

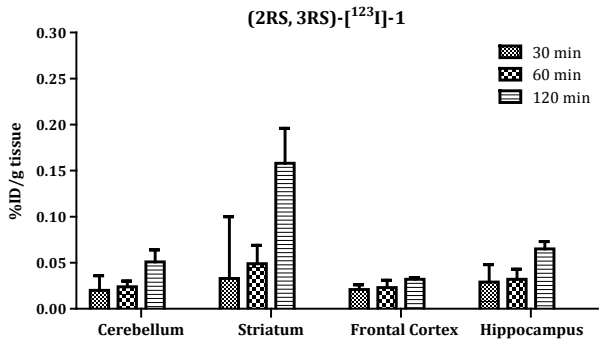

Fig. 4. Kinetic study of (2*RS*,3*RS*)-[^{123}I]-1 in the rat brain.

in the striatum then in the hippocampus, cerebellum and finally in the cortex.

When compared to cortex, hippocampus and cerebellum TACs for (2*R*,3*R*)-[^{123}I]-1, (-)-[^{125}I]-IBVM and (2*RS*,3*RS*)-[^{123}I]-1, TACs of (2*R*,3*R*)-[^{123}I]-1 were increased from 30 to 60 min then decreased from 60 to 120 min, while TACs of (2*RS*,3*RS*)-[^{123}I]-1 were increased continuously for all brain areas. By contrast, (-)-[^{125}I]-IBVM, TACs were decreased continuously. Striatal TACs were slightly increased from 30 to 60 min then decreased from 60 to 120 min p.i. for the reference compound (-)-[^{125}I]-IBVM and increased continuously for both compounds (2*R*,3*R*)-[^{123}I]-1 and (2*RS*,3*RS*)--[^{123}I]-1 (Figs. 2–4). These characteristics make the specific binding value (radioactivity ratio between the brain area of interest and cerebellum) increase over the time except the values Stri/cere for (2*R*,3*R*)--[^{123}I]-1 and Ctx/cere, Hipp/cere for (2*RS*,3*RS*)-[^{123}I]-1 (Table 1).

However, when (2*R*,3*R*)-[^{123}I]-1, (-)-[^{125}I]- IBVM and (2*RS*,3*RS*)-[^{123}I]-1 compounds are compared, the reference compound (-)-[^{125}I]-IBVM clearly showed a better *in vivo* profile since it crosses the blood-brain barrier in a much easier way (0.62% ± 0.01 ID/g tissue at 60 min p.i.) compared to (0.26% ± 0.02 ID/g at 60 min (p.i.)) for (2*R*,3*R*)-[^{123}I]-1 and (0.049% ± 0.02 ID/g at 60 min p.i.) for (2*RS*,3*RS*)-[^{123}I]-1.

By contrast, (2*R*,3*R*)-[^{123}I]-1 clearly showed a better accumulation in striatum (0.51% ID/g at 120 min p.i.) compared to 0.353% ± 0.05 ID/g for (-)-[^{125}I] IBVM and 0.158% ± 0.038 ID/g tissue for (2*RS*,3*RS*)-[^{123}I]-1. The specific binding in striatum (striatum/cerebellum) for (-)-[^{125}I]-IBVM was 2.65 at 30 min p.i. and it increased to 13 at 120 min p.i., while (2*R*,3*R*)-[^{123}I]-1 and (2*RS*,3*RS*)--[^{123}I]-1 showed their highest values of 4.74 and 3.09 at 120 min p.i, respectively.

Thyroid radioactivity was expressed as the percentage of injected dose per the whole gland as the weight of this gland is difficult to measure with precision. For tracers, a gradual increase of radioactivity during the time was observed in the thyroid gland. However, this accumulation was less for (2*RS*,3*RS*)-[^{123}I]-1 (0.033, 0.067 and 0.11% ID at 30, 60 and 120 min, respectively) compared to (2*R*,3*R*)-[^{123}I]-1 (0.21, 0.63 and 0.74% ID at 30, 60 and 120 min, respectively) and to (-)-[^{125}I]--IBVM (0.09, 0.12 and 0.19% ID at 30, 60 and 120 min, respectively) at each point of the study. These results clearly showed that the vinyl iodine-carbon bond of (2*R*,3*R*)-[^{123}I]-1 was less stable *in vivo*, compared to the aromatic bond of (-)-[^{125}I]-IBVM.

Conclusion

A vesamicol analog as a ligand for the VAChT was developed and evaluated in the rat's brain. The enantiomeric resolution of the racemic mixture (2*RS*,3*RS*)-1 showed that the analogue (2*R*,3*R*)-1 has higher specific bindings in striatum than the (2*S*,3*S*)-1 and the racemic mixture (2*RS*,3*RS*)-1. Biodistribution studies showed a good brain penetration of (2*R*,3*R*)-[^{123}I]-1. A higher level of (2*R*,3*R*)-[^{123}I]-1 was found in the striatum than in the other studied regions.

However, when compared to IBVM, (2*R*,3*R*)-[^{123}I]-1 showed higher specific binding in striatum at 120 min post injection. To determine whether (2*R*,3*R*)-[^{123}I]-1 could provide any advantage compared to IBVM, a kinetic study was realized. Even if time activity curves of (2*R*,3*R*)-[^{123}I]-1 confirmed that this compound could be used to visualize the VAChT *in vivo*, at two hours post injection.

Acknowledgment. The authors thank Prof. I. Othman, Director General and Prof. T. Yassine, Head of Chemistry Department for their support and encouragement. Thanks are also to Mr. E. Ghanem, Mr. Raffat Ajaya and Mrs. N. Karajoli for their assistance with compounds preparation and biodistribution studies.

References

1. Altar CA, Marien MR (1988) [^{3}H] Vesamicol binding in brain: autoradiographic distribution, pharmacology, and effects of cholinergic lesions. Synapse 2:486–493
2. Assaad T (2011) Synthesis and characterization of novel benzovesamicol analogs. Turk J Chem 35:189–200
3. Assaad T, Al Rayyes AH (2012) Radiosynthesis and biological evaluation of ^{123}I-(±)-trans-2-hydroxy-5-((E)--3-(iodo)allyloxy)-3-(4-phenyl-1-piperazinyl) tetralin. Nukleonika 57;1:81–85
4. Assaad T, Mavel S, Emond P *et al*. (2007) Synthesis and *ex vivo* evaluation of *aza*-trozamicol analogs as SPECT radiotracers for exploration of the vesicular acetylcholine transporter. J Labelled Compd Radiopharm 50:139–145
5. Bahr BA, Clarkson ED, Rogers GA, Noremberg K, Parsons SM (1992) A kinetic and allosteric model for the acetylcholine transporter-vesamicol receptor in synaptic vesicles. Biochemistry 31:5752–5762
6. Bahr BA, Parsons SM (1986) Demonstration of a receptor in Torpedo synaptic vesicles for the acetylcholine storage blocker L-trans-2-(4-phenyl[3,4-3H]-piperidino) cyclohexanol. Proc Natl Acad Sci USA 83:2267–2270
7. Bando K, Naganuma T, Taguchi K *et al*. (2000) Piperazine analog of vesamicol: *in vitro* and *in vivo* characterization for vesicular acetylcholine transporter. Synapse 38:27–37
8. Emond P, Mavel S, Zea-Ponce Y *et al*. (2007) (E)-[^{125}I]--5-AOIBV: a SPECT radioligand for thevesicular acetylcholine transporter. Nucl Med Biol 34:967–971
9. Jung YW, Frey KA, Mulholland GK *et al*. (1996) Vesamicol receptor mapping of brain cholinergic neurons with radioiodine-labeled positional isomers of benzovesamicol. J Med Chem 39:3331–3342
10. Jung YW, Van Dort ME, Gildersleeve DL, Wieland DM (1990) A radiotracer for mapping cholinergic neurons of the brain. J Med Chem 33:2065–2068

11. Kuhl DE, Minoshima S, Fessler JA *et al*. (1996) *In vivo* mapping of cholinergic terminals in normal aging, Alzheimer's disease and Parkinson's disease. Ann Neurol 40:399–410
12. Mesulam MM, Mufson EJ, Levey AI, Wainer AI (1983) Cholinergic innervations of cortex by the basal forebrain: cytochemistry and cortial connection of septal area, diagonal band nuclei, nucleus basalis 9 substantia innominata) and hypothalamus in the rhesus monkey. J Comp Neurol 214:170–197
13. Mulholland GK, Jung YW (1992) Improved synthesis of [^{11}C]methylamino-benzovesamicol. J Labelled Compd Radiopharm 31:253–259
14. Mulholland GK, Jung YW, Wieland DM, Kilbourn MR, Kuhl DE (1993) Synthesis of [^{18}F]-fluoroethoxybenzovesamicol, a radiotracer for cholinergic neurons. J Labelled Compd Radiopharm 33:589–591
15. Parsons SM, Bahr BA, Rogers GA, Clarkson ED, Noremberg K, Hicks BW (1993) Acetylcholine transporter-vesamicol receptor pharmacology and structure. Prog Brain Res 98:175–181
16. Rogers GA, Parsons SM, Anderson DC *et al*. (1989) Synthesis, *in vitro* acetylcholine-storage-blockingactivities, and biological properties of derivatives and analogues of trans-2-(4-phenylpiperidino) cyclohexanol (vesamicol). J Med Chem 32:1217–1230
17. Sorger D, Schliebs R, Kampfer I *et al*. (2000) *In vivo* [^{125}I]--iodobenzovesamicol binding reflects cortical cholinergic deficiency induced by specific immunolesion of rat basal forebrain cholinergic system. Nucl Med Biol 27:23–31
18. Van Dort ME, Jung YW, Gildersleeve DL, Hagen CA, Kuhl DE, Wieland DM (1993) Synthesis of the ^{123}I- and ^{125}I-labeled cholinergic nerve marker (-)-5-iodobenzovesamicol. Nucl Med Biol 20:929–37
19. Whitehouse P, Price DL, Stribble RG *et al*. (1982) Alzheimer's disease and senile dementia: loss of neurons in basal forebrain. Science 215:1237–1239
20. Zea-Ponce Y, Mavel S, Assaad T *et al*. (2005) Synthesis and *in vitro* evaluation of new benzovesamicol analogues as potential imaging probes for the vesicular acetylcholine transporter. Bioorg Med Chem 13:745–753